

## PDF hosted at the Radboud Repository of the Radboud University Nijmegen

The following full text is a publisher's version.

For additional information about this publication click this link.

<http://hdl.handle.net/2066/98901>

Please be advised that this information was generated on 2016-01-22 and may be subject to change.

# Infrared-Induced Reactivity of N<sub>2</sub>O on Small Gas-Phase Rhodium Clusters

Suzanne M. Hamilton,<sup>†</sup> W. Scott Hopkins,<sup>†</sup> Dan J. Harding,<sup>§</sup> Tiffany R. Walsh,<sup>‡,||</sup> Marko Haertelt,<sup>§</sup> Christian Kerpel,<sup>§</sup> Philipp Gruene,<sup>§</sup> Gerard Meijer,<sup>§</sup> André Fielicke,<sup>\*,§</sup> and Stuart R. Mackenzie<sup>\*,†</sup>

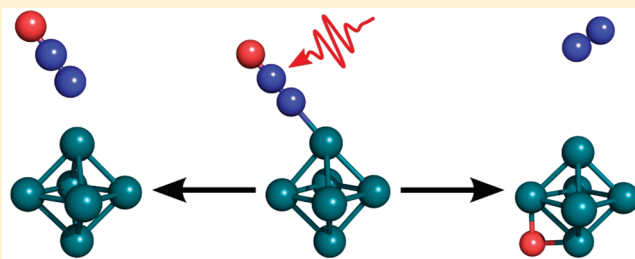
<sup>†</sup>Department of Chemistry, Physical and Theoretical Chemistry Laboratory, University of Oxford, South Parks Road, Oxford, OX1 3QZ, U.K.

<sup>‡</sup>Department of Chemistry, University of Warwick, Coventry, CV4 7AL, U.K.

<sup>§</sup>Fritz-Haber-Institut der Max-Planck-Gesellschaft, Faradayweg 4-6, D-14195 Berlin, Germany

<sup>||</sup>Centre for Scientific Computing, University of Warwick, Coventry, CV4 7AL, U.K.

**ABSTRACT:** Far- and mid-infrared multiple photon dissociation spectroscopy has been employed to study both the structure and surface reactivity of isolated cationic rhodium clusters with surface-adsorbed nitrous oxide, Rh<sub>n</sub>N<sub>2</sub>O<sup>+</sup> ( $n = 4-8$ ). Comparison of experimental spectra recorded using the argon atom tagging method with those calculated using density functional theory (DFT) reveals that the nitrous oxide is molecularly bound on the rhodium cluster via the terminal N-atom. Binding is thought to occur exclusively on atop sites with the rhodium clusters adopting close-packed structures. In related, but conceptually different experiments, infrared pumping of the vibrational modes corresponding with the normal modes of the adsorbed N<sub>2</sub>O has been observed to result in the decomposition of the N<sub>2</sub>O moiety and the production of oxide clusters. This cluster surface chemistry is observed for all cluster sizes studied except for  $n = 5$ . Plausible N<sub>2</sub>O decomposition mechanisms are given based on DFT calculations using exchange-correlation functionals. Similar experiments pumping the Rh–O stretch in Rh<sub>n</sub>ON<sub>2</sub>O<sup>+</sup> complexes, on which the same chemistry is observed, confirm the thermal nature of this reaction.



## INTRODUCTION

Reactions on practical transition metal catalysts often occur not on pristine perfect crystal surfaces but on steps and defect sites.<sup>1</sup> To investigate the geometric and electronic factors determining the reactivity of these surface structures, small gas-phase clusters are frequently used as model systems as they are more amenable to experimental and computational study than the more complex surface. Such cluster studies are themselves challenging, however, owing to the strong dependence of many of the chemical and physical properties of these systems on their size and structure. For example, in the case of charged rhodium clusters (one such catalytically interesting metal)<sup>2</sup> different cluster forms, either of electronic and/or geometric origin, appear to greatly influence the reactivities. In reactions of Rh<sub>n</sub><sup>±</sup> clusters under single collision conditions using Fourier transform ion cyclotron resonance mass spectrometry, the unusual kinetics observed for some cluster sizes have been interpreted as arising from the presence of multiple isomeric forms or electronic states with significantly different rates of reaction.<sup>3</sup> In other experiments the rates of reaction of particular Rh<sub>n</sub><sup>±</sup> clusters have been observed to differ dramatically from those of adjacent sizes, often by several orders of magnitude.<sup>4,5</sup> This is exemplified by the Rh<sub>n</sub><sup>±</sup> + N<sub>2</sub>O reaction, which has shown  $n = 5, 19$ , and  $28$  to have anomalously low reactivity, up to 2 orders of magnitude lower

than adjacent clusters.<sup>6</sup> Such non-monotonic variation in reactivity with cluster size has been an area of intense interest and a focal point for research in many related systems.<sup>7,8</sup>

To aid in the interpretation of experimental observations, numerous computational studies involving bare and decorated rhodium clusters have been undertaken. Early theoretical investigations on rhodium clusters were driven by the observation of unusually large magnetic moments and their potential technological applications,<sup>9-11</sup> but more recent attempts have sought to account for reactivity trends in terms of the underlying geometrical structure.<sup>12,13</sup> As multireference calculations are possible only for the very smallest clusters,<sup>14</sup> density functional theory (DFT) is a commonly used tool to efficiently describe the electronic structures of larger clusters.<sup>15</sup> Many groups have applied DFT to rhodium clusters, but within this literature there is disagreement over whether the basic structural units are open cubic motifs<sup>16,17</sup> or close-packed polytetrahedra.<sup>18,19</sup>

One major concern in investigating transition metal clusters computationally is the poorly understood role that electron exchange and correlation effects play in determining chemical

Received: February 4, 2011

Revised: February 18, 2011

Published: March 10, 2011

and physical properties. This is a particular problem in high-spin systems such as those found for rhodium clusters. For example, Wang and Johnson showed that, in the case of the  $\text{Ru}_4$  cluster, the inclusion of a fraction of exact Hartree–Fock (HF) exchange changed the predicted global minimum from an open, planar structure to a close-packed tetrahedron.<sup>20</sup> A similar effect is observed in rhodium clusters, where the fraction of HF exchange heavily influences the relative energetic ordering of the cubic and close-packed motifs. The question as to which geometric arrangement is adopted by ground-state  $\text{Rh}_n^+$  clusters was recently addressed experimentally using (far-)infrared multiple photon dissociation (IR-MPD) spectroscopy.<sup>21,22</sup> The vibrational spectra of cationic rhodium clusters provided evidence that close-packed structures are favored over open, cubic motifs.<sup>21</sup>

In related IR-MPD studies of decorated rhodium clusters, we have recently shown that where  $\text{N}_2\text{O}$  is molecularly bound to a  $\text{Rh}_6^+$  cluster, surface decomposition can be thermally induced by pumping the  $\text{N}_2\text{O}$  vibrational modes with intense infrared radiation.<sup>23</sup> Here, we report the results of IR-MPD studies of  $\text{Rh}_n\text{N}_2\text{O}^+$  ( $4 \leq n \leq 8$ ) complexes in both the mid-infrared (covering vibrational transitions in the  $\text{N}_2\text{O}$  moiety) and far-infrared (metal–metal vibrations) regions. The resulting spectra are interpreted with the aid of DFT calculations.

## EXPERIMENTAL DETAILS

All experiments were carried out at the Free Electron Laser for Infrared eXperiments (FELIX)<sup>24</sup> facility in the Netherlands using an experimental apparatus described previously.<sup>25–27</sup> Two conceptually different experiments have been performed. IR-MPD experiments of argon atom tagged  $\text{Rh}_n\text{N}_2\text{O}^+$  clusters yield information on the cluster structures and the nature of the  $\text{N}_2\text{O}$  binding. Following cluster characterization, the surface reactivity of untagged  $\text{Rh}_n\text{N}_2\text{O}^+$  complexes was investigated by heating the cluster via the  $\text{N}_2\text{O}$  vibrational modes to induce thermal decomposition.

Rhodium cluster cations are generated in a laser ablation source. An intense pulse of helium seeded with argon (ca. 0.3%) cools the plasma and carries it through a cryogenically cooled reaction channel held at 173 K. A late-mixing valve admits  $\text{N}_2\text{O}$  directly into the reaction channel to let the  $\text{N}_2\text{O}$  interact with the clusters before the expansion of the molecular beam into vacuum. The beam of cationic clusters, some of which are complexed with one or more adsorbed  $\text{N}_2\text{O}$  molecules and argon atoms, passes through a skimmer and a 1 mm diameter aperture into the extraction region of a reflectron time-of-flight mass spectrometer. On alternate shots, the molecular beam is overlapped with the counter-propagating (ca. 20 mJ/pulse) infrared beam from the FELIX light source. When resonant with an allowed transition within an argon-tagged cluster, the infrared radiation is absorbed, heating the cluster via intramolecular vibrational redistribution (IVR), ultimately resulting in the loss of the argon atom. Comparison of the mass spectra recorded in the presence and absence of the infrared beam provides the depletion as a function of excitation wavelength and permits an infrared action spectrum to be recorded. In this work, spectra are recorded between 100 and  $2350\text{ cm}^{-1}$ , covering the region from the low-frequency metal–metal modes up to the higher frequency stretching modes of the  $\text{N}_2\text{O}$  moiety.

For the reactivity studies, pure helium is used as the carrier gas to avoid the unnecessary complications of co-adsorbed argon atoms. The  $\text{N}_2\text{O}$  binding energy to  $\text{Rh}_n^+$  is apparently greater

than that of Ar, as in these experiments it is not necessary to cryogenically cool the cluster channel, which is held at 308 K. As our interest lies in driving surface reactions following infrared absorption, spectra are recorded only in the region of the  $\text{N}_2\text{O}$  vibrational modes, which are denoted according to those of free  $\text{N}_2\text{O}$ , namely,  $\nu_1$  (N–O stretch) from  $1250$  to  $1380\text{ cm}^{-1}$ ,  $\nu_2$  (bend), from  $510$  to  $620\text{ cm}^{-1}$ , and  $\nu_3$  ( $\text{N}\equiv\text{N}$  stretch) from  $2190$  to  $2340\text{ cm}^{-1}$ .

## COMPUTATIONAL DETAILS

In support of the experimental work, calculations of cluster structures and reaction pathways were carried out at the level of density functional theory using the Turbomole 6.1 package.<sup>28</sup> A range of structures were considered for each of the naked rhodium cluster sizes, based on structures determined previously by a combination of basin hopping and DFT.<sup>21</sup> The structures were reoptimized with  $\text{N}_2\text{O}$  placed on the surface in a range of atop, bridged, and high coordination sites as well as a range of dissociated geometries. Normal mode analyses were performed to ensure that all structures were minima on the potential energy surface and to provide the vibrational mode frequencies for comparison with the experimental spectra. In determination of likely reaction pathways, eigenvector-following was used to locate transition state structures along the reaction pathway.<sup>29,30</sup>

Our previous IR-MPD work on naked rhodium clusters has suggested that pure generalized gradient approximation (GGA) functionals are unsuitable for rhodium clusters, and inclusion of a fraction of HF exchange (in the form of a hybrid functional) is required to correctly predict the relative energetic ordering of isomers as inferred from experimental observations.<sup>21</sup> GGA functionals are also known to systematically underestimate barrier heights to reactions on metal cluster surfaces.<sup>31</sup> Accordingly, we have performed calculations with two different hybrid functionals, PBE0<sup>32</sup> (25% HF exchange) and the hybrid meta-functional TPSSH<sup>33</sup> (10% HF exchange), which is based on the TPSS functional that, in past studies, has yielded good agreement with experiment.<sup>34</sup> Compared to many other common GGA and hybrid functionals, TPSSH has previously been shown to reproduce transition metal–ligand bond dissociation energies more consistent with experimental results, which is especially important in this study.<sup>35</sup> Even so, Jensen found TPSSH to yield mean absolute errors of 0.38 eV in the diatomic binding energies of second-row transition metal atoms to p-block elements.<sup>35</sup> For consistency, the def2-TZVP basis sets were used for all elements.<sup>36,37</sup> This was found to be a large enough basis to calculate accurate transition metal–ligand bond dissociation energies,<sup>35</sup> and has previously been applied successfully to the prediction of  $\text{Rh}_n(\text{CO})_m^+$  IR spectra.<sup>38</sup> No shift has been applied to the calculated spectra reported here.

## RESULTS AND DISCUSSION

**A. Spectroscopy Overview.** The IR-MPD spectra of  $\text{Rh}_n\text{N}_2\text{OAr}^+$ , recorded for  $4 \leq n \leq 8$ , are shown in Figure 1. In each case the spectra comprise intense bands in the mid-infrared and weaker bands below  $\sim 500\text{ cm}^{-1}$ . The intense absorption bands all lie within  $50\text{ cm}^{-1}$  of the vibrational wavenumbers for the normal modes of free  $\text{N}_2\text{O}$ ,<sup>39</sup> demonstrating conclusively that the ligand is molecularly bound on the surface of the cluster. The IR-MPD spectra of argon-tagged  $\text{Rh}_n\text{O}^+$  clusters, formed by reactions in the cluster source, were

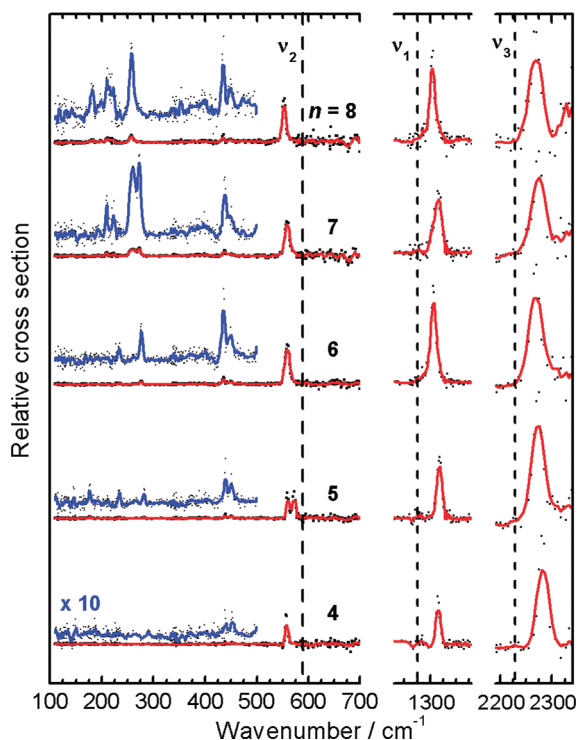


**Figure 1.** IR-MPD spectra of argon-tagged  $\text{Rh}_n\text{N}_2\text{O}^+$  ( $n = 4–8$ ) complexes. The strong absorptions observed close to those of free  $\text{N}_2\text{O}$  (indicated by dashed lines) indicate molecular rather than dissociative adsorption. The weaker absorptions at lower wavenumber arise from metal–metal and metal–ligand vibrational modes.

recorded simultaneously and exhibit the expected strong absorptions due to Rh–O stretch vibrations around  $600\text{ cm}^{-1}$ . Importantly, these transitions are absent in the  $\text{Rh}_n\text{N}_2\text{OAr}^+$  spectra, allowing us to rule out complications arising from dissociative  $\text{N}_2\text{O}$  adsorption producing coadsorbed O and  $\text{N}_2$ .

The observation of molecularly adsorbed  $\text{N}_2\text{O}$  on rhodium clusters is initially somewhat surprising. Under single collision conditions in mass spectrometry studies, the only products of collisions between  $\text{Rh}_n^+$  and  $\text{N}_2\text{O}$  were oxide clusters; no  $\text{Rh}_n\text{N}_2\text{O}^+$  product peaks were observed.<sup>6</sup> Here,  $\text{Rh}_n\text{N}_2\text{O}^+$  clusters are formed in the comparatively high pressure environment of the reaction channel, suggesting that three-body collisions with the carrier gas efficiently stabilize the molecularly bound  $\text{N}_2\text{O}$  complex. This stabilization occurs not only at 173 K in the argon tagging experiments, but also on room temperature clusters in the absence of argon. The stability of the  $\text{Rh}_n\text{N}_2\text{O}^+$  complex at room temperature marks something of a contrast with nitrous oxide binding on extended rhodium surfaces where it is known to decompose at temperatures as low as 95 K on some crystal planes.<sup>40,41</sup>

#### B. Spectrum in the Region of the $\text{N}_2\text{O}$ Vibrational Modes.

As well as signifying molecular adsorption, the IR-MPD spectra in the region of the  $\text{N}_2\text{O}$  vibrational modes reveal important further information on the nature of the  $\text{N}_2\text{O}$  binding. For each cluster size, the bands identifiable with the two  $\text{N}_2\text{O}$  stretches,  $\nu_1$  (nominally the N–O stretch;  $\sim 1320\text{ cm}^{-1}$ ) and  $\nu_3$  (N≡N stretch;  $\sim 2250\text{ cm}^{-1}$ ), occur at higher wavenumbers than the equivalent transitions in free  $\text{N}_2\text{O}$  (marked in Figure 1 by the dashed lines). By contrast, the fundamental in the bending mode,  $\nu_2$  ( $\sim 560\text{ cm}^{-1}$ ), is notably red-shifted with respect to that in free  $\text{N}_2\text{O}$ . These observations are consistent with the vibrations

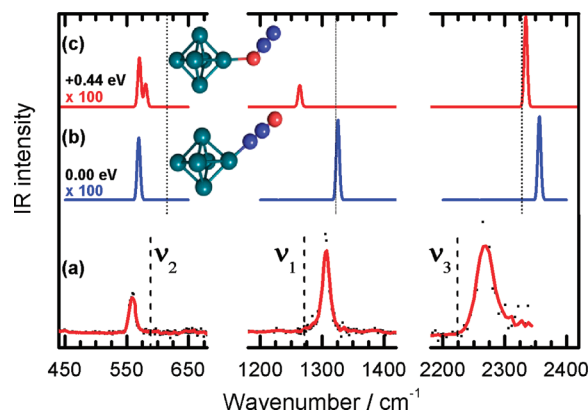


**Figure 2.** (a) Experimental IR-MPD spectrum of the argon-tagged  $\text{Rh}_6\text{N}_2\text{O}^+$  complex. (b, c) Unscaled calculated spectra of the lowest lying isomers of N-bound and O-bound  $\text{Rh}_6\text{N}_2\text{O}^+$  complexes. The two stretches,  $\nu_1$  and  $\nu_3$ , are measured to be notably blue-shifted and the bending mode,  $\nu_2$ , red-shifted relative to the experimental free  $\text{N}_2\text{O}$  (dashed lines). The observed shifts, particularly  $\nu_1$ , match well with the calculated spectrum of the N-bound cluster (b). Dotted lines mark the free  $\text{N}_2\text{O}$  vibrational wavenumbers as calculated using TPSSh/TZVP. Calculated spectra in the  $\nu_2$  region are very weak and have been multiplied by 100 for clarity.

in  $\text{N}_2\text{O}$  adsorbed on extended  $\text{Ru}(001)$ ,<sup>42</sup>  $\text{Pt}(111)$ ,<sup>43</sup> and  $\text{Pd}(110)$ <sup>44</sup> surfaces and have been ascribed to binding via the terminal N atom. Conversely,  $\text{N}_2\text{O}$  binding on  $\text{ZnO}$ <sup>45</sup> and  $\text{TiO}_2(110)$ <sup>46</sup> surfaces occurs via the metal center and terminal O atom as indicated by a significant red shift of the N–O stretch from its free  $\text{N}_2\text{O}$  value.

To further test the likely binding orientation, we have calculated a range of low-lying  $\text{Rh}_6\text{N}_2\text{O}^+$  structures with different  $\text{N}_2\text{O}$  binding geometries using the TPSSh functional (see Figure 2). For simplicity, each structure was based on the dectet spin-state ( $2S + 1 = 10$ ) of the octahedral  $\text{Rh}_6^+$  cluster geometry previously calculated to be the lowest energy structure.<sup>12,21</sup> Consistent with the spectroscopy discussed above, the lowest-lying isomer identified has  $\text{N}_2\text{O}$  linearly bound on an atop site, via the terminal N atom. We have also identified a real minimum on the potential energy landscape corresponding to the O-bound complex, again in an atop configuration, but this lies some 0.4 eV above the minimum energy structure.

We can further compare the calculated spectra for the low-lying isomers identified by DFT with the experimental IR-MPD spectra shown in Figure 1. For both the N-bound and O-bound complexes, the normal modes of the adsorbed  $\text{N}_2\text{O}$  lie close to those of the free molecule. The clearest evidence for N-binding is observed in the region of the  $\nu_1$  mode (N–O stretch). Experimentally, this cluster band is observed ca.  $30\text{ cm}^{-1}$  blue-shifted from that of free  $\text{N}_2\text{O}$ . This is consistent with the predicted spectrum in Figure 2b for the N-bound complex, which also shows this band slightly blue-shifted from the calculated free  $\text{N}_2\text{O}$  transition. By contrast, the calculated spectrum of the O-bound complex predicts a  $60\text{ cm}^{-1}$  red shift of the  $\nu_1$  band.

Several structures were also optimized with  $\text{N}_2\text{O}$  occupying two atom bridging sites. This type of binding, however, breaks one of the  $\text{N}_2\text{O}$   $\pi$ -bonds, and results in shifts in the  $\text{N}_2\text{O}$  stretching modes of several hundred  $\text{cm}^{-1}$ , far larger than the small shifts observed in the IR-MPD spectra. There is no evidence in the observed spectra to support  $\text{N}_2\text{O}$  binding to anything other than atop sites.



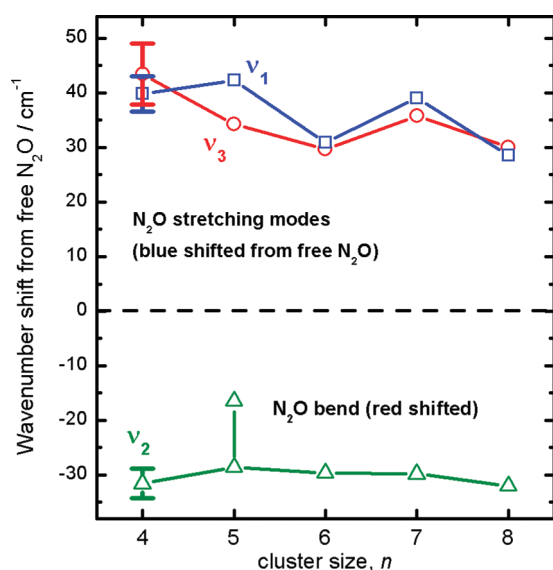


**Figure 3.** Experimentally observed shifts in the vibrational wavenumbers of  $\text{N}_2\text{O}$  (cluster-free  $\text{N}_2\text{O}$ ) adsorbed on cationic rhodium clusters. The peak centers were extracted by fitting the spectral features to Gaussian line shape profiles. The FELIX spectral bandwidth is typically  $\sim 0.5\%$  of the wavelength and represents the largest uncertainty in these observations.

The  $\text{Rh}_n\text{N}_2\text{O}^+$  vibrational spectra predicted by PBE0/TZVP are in slightly better agreement with the experimental data than those determined with TPSSH:  $\nu_1$  is shifted  $33\text{ cm}^{-1}$  higher than free  $\text{N}_2\text{O}$ , in good agreement with the  $30\text{ cm}^{-1}$  shift observed by IR-MPD. PBE0/TZVP also favors more symmetrical  $\text{N}_2\text{O}$  binding sites, which preserve the degeneracy of the  $\text{N}_2\text{O}$  bend, consistent with the experimental spectra of  $n = 4, 6, 7$ , and  $8$ . We nevertheless use TPSSH because of its superior performance in the reactivity calculations discussed below, in which PBE0 fails qualitatively to describe the outcome of the reaction.

Figure 3 summarizes the observed spectral shifts from free  $\text{N}_2\text{O}$  transitions for all clusters studied here,  $4 \leq n \leq 8$ . Although these shifts vary somewhat with increasing cluster size, indicating their sensitivity to the underlying structure, the sign of the shifts for each vibrational mode is common to all clusters indicating that  $\text{N}_2\text{O}$  is N-bound on each of these clusters; see above. In the  $\text{N}_2\text{O}$  bend region of the  $n = 5$  cluster, two distinct peaks are observed that are separated by  $18\text{ cm}^{-1}$ . While we cannot rule out the possible presence of two isomeric forms of  $\text{Rh}_5\text{N}_2\text{O}^+$  (different  $\text{N}_2\text{O}$  binding sites or different metal structural motifs), this appears improbable as no multiple peaks are observed in either of the  $\text{N}_2\text{O}$  stretching regions. Instead, calculations suggest this splitting arises due to the lifting of the degeneracy of the two  $\text{N}_2\text{O}$  bending modes when the  $\text{N}_2\text{O}$  binds to a site without high symmetry.

**C. Infrared-Driven Cluster Surface Reactivity.** The observation of transitions associated with vibrational modes in  $\text{N}_2\text{O}$  in the spectra of  $\text{Rh}_n\text{N}_2\text{OAr}^+$  clusters is proof that the  $\text{N}_2\text{O}$  is molecularly adsorbed on the metal cluster surface. In an earlier communication we showed that by pumping such a mode in  $\text{Rh}_6\text{N}_2\text{OAr}^+$ , it is possible to heat the complex sufficiently to drive surface decomposition producing the  $\text{Rh}_6\text{O}^+$  oxide cluster.<sup>23</sup>

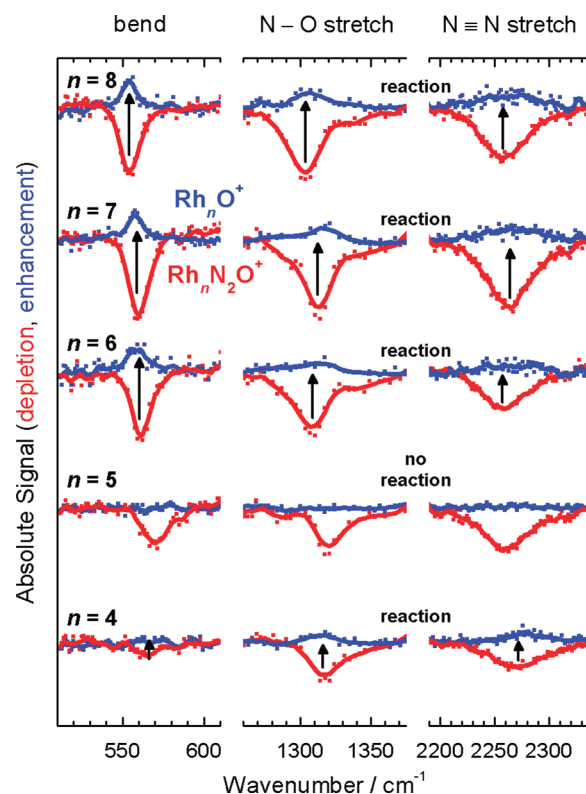
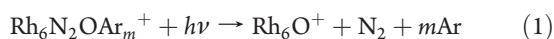


**Figure 4.** Infrared-driven cluster surface reactivity. Pumping  $\text{N}_2\text{O}$  vibrational modes in  $\text{Rh}_n\text{N}_2\text{O}^+$  (red curves) results in both  $\text{N}_2\text{O}$  loss and surface-induced dissociation, which leads to concomitant increases in  $\text{Rh}_n\text{O}^+$  signals (blue curves). The only exception is  $n = 5$ , which exhibits no apparent oxide enhancement.

Furthermore, this reaction was shown to be a significant channel in addition to the usual  $\text{N}_2\text{O}$  loss. In terms of the reactivity, the presence of the Ar atoms is an unnecessary complication and thus we have extended these studies to the cluster range  $n = 4-8$  without the rare gas tagging. In the spectral region of the  $\text{N}_2\text{O}$  vibrational modes, the IR-MPD spectra (now observed in the  $\text{N}_2\text{O}$  loss channel) were essentially identical to those discussed above in the rare gas tagging experiments with the exception of broader line width, resulting from both the increased FEL bandwidth employed in these studies and the higher internal energies of the clusters, which were generated without cryogenic cooling of the cluster channel.

Figure 4 shows the IR-MPD spectra of  $\text{Rh}_n\text{N}_2\text{O}^+$  ( $n = 4-8$ ) in the region of fundamental transitions of each of the three  $\text{N}_2\text{O}$  vibrational modes. In each case, the signal in the carrier ion channel ( $\text{Rh}_n\text{N}_2\text{O}^+$ , red lines) and the corresponding oxide cluster channel ( $\text{Rh}_n\text{O}^+$ , blue lines) are shown. Similar spectra were recorded for larger clusters, but low signal-to-noise prevented their detailed analysis. In these studies, no depletion of  $\text{Rh}_n\text{N}_2\text{O}^+$  was observed on smaller clusters,  $n \leq 3$ .

With the notable exception of the  $n = 5$  cluster, each depletion in the  $\text{Rh}_n\text{N}_2\text{O}^+$  signal is accompanied by an *enhancement* in the  $\text{Rh}_n\text{O}^+$  intensity at the same wavenumber. In principle, the latter could arise from direct  $\text{N}_2\text{O}$  loss from  $\text{Rh}_n\text{O}(\text{N}_2\text{O})^+$ , whose spectrum in these regions is similar to  $\text{Rh}_n\text{N}_2\text{O}^+$ . However, the source conditions were optimized such that very little  $\text{Rh}_n\text{O}(\text{N}_2\text{O})^+$  was produced by the laser ablation source, and its depletion accounts, at most, for a small fraction of the overall

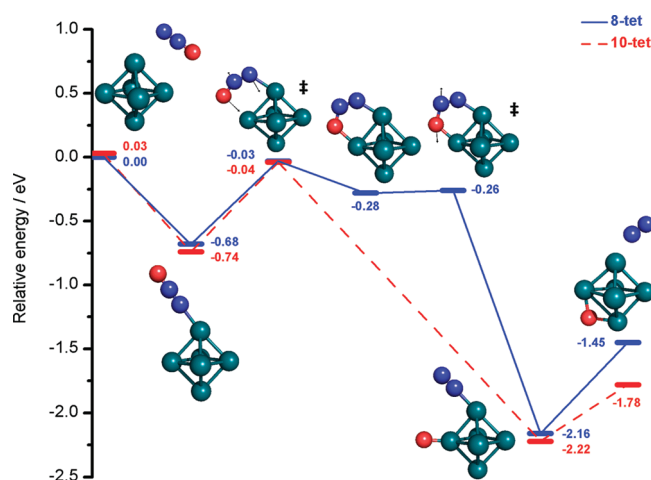


**Figure 5.** Calculated reaction profiles for the infrared induced cluster surface decomposition of  $\text{N}_2\text{O}$  on  $\text{Rh}_6^+$ . All energies are given relative to the bare octet  $\text{Rh}_6^+$  cluster +  $\text{N}_2\text{O}$  limit. The binding energy of molecular  $\text{N}_2\text{O}$  to the cluster is slightly higher in energy than the largest barrier to reaction. Arrows indicate the transition vector at each transition state. The product energies indicated include the free  $\text{N}_2$  energy.

cluster oxide signal enhancement. Instead, we believe that thermally induced decomposition of the  $\text{N}_2\text{O}$  on the cluster surface is the source of the oxide signal: The surface bound  $\text{N}_2\text{O}$  moiety acts as a chromophore absorbing infrared radiation via excitation of its vibrational modes. This energy is then rapidly transferred via IVR to the substrate metal framework with the effect of heating the whole cluster. By analogy with temperature-programmed desorption/reactivity on extended surfaces, the system is eventually promoted over the barrier to surface reactivity, resulting in dissociation of the  $\text{N}_2\text{O}$  component and the subsequent desorption of molecular nitrogen.

Intriguingly, this reaction is not observed for any  $\text{N}_2\text{O}$  mode in  $n = 5$ . There is nothing anomalous in the IR-MPD spectrum of  $\text{Rh}_5\text{N}_2\text{O}^+$ , but no detectable enhancement in  $\text{Rh}_5\text{O}^+$  fragment ions results. The loss channel in this case appears to be simple  $\text{N}_2\text{O}$  desorption, but the corresponding enhancement in the naked  $\text{Rh}_5^+$  signal could not be detected above the large background of bare clusters. Interestingly,  $\text{Rh}_5^+$  has also been observed as anomalously unreactive in reactivity studies with  $\text{N}_2\text{O}$  under single collision conditions<sup>6</sup> (and indeed with small alkanes<sup>4</sup>). While the nature of the activation is fundamentally different here (infrared excitation rather than collision energy), the same reaction apparently occurs in both cases. The ratio of the absolute  $\text{Rh}_n\text{O}^+$  signal enhancement to the depletion in the  $\text{Rh}_n\text{N}_2\text{O}^+$  signal provides a measure of the branching ratio for the surface reaction ( $\text{Rh}_n\text{O}^+ + \text{N}_2$ ) versus  $\text{N}_2\text{O}$  desorption. For all clusters, except  $\text{Rh}_5^+$ , the gain in the oxide signal only accounts for at most around one-third of the total depletion in the  $\text{Rh}_n\text{N}_2\text{O}^+$  signal implying that at least one other pathway—in all probability the direct desorption of  $\text{N}_2\text{O}$ —competes effectively with this channel.

We have investigated plausible mechanisms for the cluster surface decomposition of  $\text{N}_2\text{O}$  using DFT and have employed the eigenvector following method to identify pertinent structures along potential reaction pathways. We have concentrated on the  $\text{Rh}_6\text{N}_2\text{O}^+$  cluster although the efficacy of qualitatively similar reaction pathways on other cluster sizes has been confirmed. The (terminal N-atom) binding energy of  $\text{N}_2\text{O}$  to the octet and

dectet spin states of  $\text{Rh}_6^+$  cluster is calculated using the TPSSH functional to be 0.68 and 0.77 eV, respectively. Direct dissociation of O-bound  $\text{N}_2\text{O}$  can be discounted on two grounds: First,  $\text{N}_2\text{O}$  is found to be N-bound on the basis of the infrared shifts, as discussed above and yet the product is an oxide cluster,  $\text{Rh}_6\text{O}^+$ . Second, the reaction pathway for the O-bound complex involves a markedly larger ( $>1.1$  eV) reaction barrier which is almost certainly higher than the  $\text{N}_2\text{O}$  binding energy. We conclude, therefore, that the reaction pathway involves a considerable rearrangement of the molecule resulting in the O atom binding to the cluster.

Figure 5 shows one calculated reaction pathway involving the lowest-lying transition states identified. Both the octet and dectet pathways are given, since they are energetically very similar and could possibly interconvert via a two-state reaction mechanism.<sup>47</sup> The highest barrier to reaction is the initial surface rearrangement of the  $\text{N}_2\text{O}$ , bending the adsorbed molecule to bring the O atom toward an adjacent Rh atom. Once this barrier is overcome, the  $\text{N}_2\text{O}$  dectet cluster dissociates immediately. The octet pathway proceeds via a bridged intermediate minimum and a second, lower-lying transition state in which the N–O bond is broken.

Clearly, this surface reaction must compete with the simple  $\text{N}_2\text{O}$  desorption channel. For both spin states, the calculated reaction barrier lies less than 0.1 eV lower than the  $\text{N}_2\text{O}$  binding energy; therefore DFT finds these two processes to be effectively isoenergetic. In all probability, however, where energetically possible the rate of desorption is likely to be much larger than the rate of reaction, since reaction requires specific rearrangement of the  $\text{N}_2\text{O}$  for the oxygen atom to bind to the metal cluster and therefore exhibits a much smaller density of states in the transition structure. Conversely, the fact that the surface reaction is observed at all indicates that the barrier to reaction is lower than the  $\text{N}_2\text{O}$  surface binding energy, as otherwise desorption would occur every time.

The reaction pathway shown in Figure 5 is qualitatively similar to that determined using the hybrid functional PBE0.<sup>23</sup> In our spectroscopic work on bare rhodium metal clusters, the PBE0 functional was shown to significantly improve the prediction of cluster structures as determined from IR-MPD spectra.<sup>21</sup> As discussed earlier, the frequencies of the  $\text{N}_2\text{O}$  modes are better predicted by PBE0 than by TPSSH. However, Table 1 shows that the reaction barrier calculated using PBE0 is significantly larger than the cluster– $\text{N}_2\text{O}$  binding energy which would preclude the surface dissociation channel. PBE, a GGA functional included for comparison, predicts an even higher binding energy of 0.83 eV, while the reaction barrier is lowered to 0.51 eV. While this is consistent with the observed reaction, PBE, although determining the correct structural motif (distorted octahedral) predicts a calculated spectrum whose agreement with experiment is very poor. The difficulty in identifying a completely ideal functional is not entirely unexpected as density functionals are usually developed for treating main group chemistry. Indeed, functional validation is usually performed on metal atoms with main group ligands or even on bulk metals.<sup>15</sup> Given that it is exactly because the electronic structure of small clusters differ so markedly from those of the corresponding bulk metal that makes them chemically interesting, it is unsurprising that these functionals are less well able to describe the properties (structures, reactivities, etc.) of transition metal clusters. This is particularly true for high-spin systems such as the current one, hence the sensitivity of our results on the description of the exchange contribution. In this case, while PBE0 produces the best agreement with experimental

**Table 1.** Comparison of Calculated Reaction Barrier Heights and Binding Energies Using Functionals with Varying Proportions of Exact Exchange<sup>a</sup>

functional	% HF exchange	(2S + 1)	maximum reaction barrier/eV	Rh <sub>6</sub> <sup>+</sup> –N <sub>2</sub> O binding energy/eV
PBE	0	8	0.51	0.83
TPSSH	10	8	0.65	0.68
TPSSH	10	10	0.70	0.77
PBE0	25	10	0.79	0.66

<sup>a</sup>For PBE and PBE0, the lowest spin isomer is listed. Both the octet and dectet clusters in TPSSH are included because their difference in energy is only 0.03 eV.

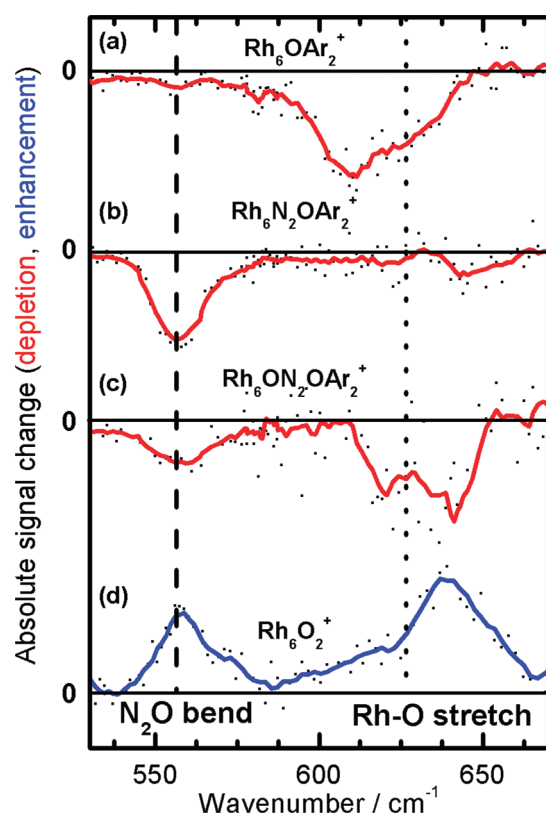


**Figure 6.** Depletion spectra of (a) Rh<sub>6</sub>OAr<sub>2</sub><sup>+</sup>, (b) Rh<sub>6</sub>N<sub>2</sub>OAr<sub>2</sub><sup>+</sup>, and (c) Rh<sub>6</sub>ON<sub>2</sub>OAr<sub>2</sub><sup>+</sup>. The last of these shows two peaks corresponding to the N<sub>2</sub>O bend and O stretch (blue-shifted by ca. 20 cm<sup>−1</sup> due to the coadsorbed N<sub>2</sub>O molecule), implying that this species comprises an oxygen atom and N<sub>2</sub>O molecule separately bound to the cluster surface. The spectrum of Rh<sub>6</sub>O<sub>2</sub><sup>+</sup> (d), recorded in the absence of argon tagging, shows enhancements following pumping of each vibrational mode.

structures of Rh<sub>n</sub>N<sub>2</sub>O<sup>+</sup>, TPSSH apparently represents a better overall compromise for geometric and thermodynamic properties.

Regardless of which functional is used to predict the reaction pathway, our calculations indicate that absorption of several photons is required to overcome the barrier: a minimum of 4, 10, and 3 when the infrared is on-resonance with  $\nu_1$ ,  $\nu_2$ , and  $\nu_3$ , respectively, using the barrier heights predicted at the TPSSH/def2-TZVP level of theory. This assumes that the energy from all of the absorbed photons is redistributed into the normal mode involved in the reaction, so in practice a considerably larger number of photons would be necessary to overcome the barrier on the time scale of the experiment. The intense infrared pulse energies delivered by FELIX, up to a maximum of ca. 50 mJ per macropulse, makes this multiple-photon process possible.

The moderate fluence of each micropulse and relatively long duration of the macropulse mean the photon absorption is likely to be sequential, with the energy being transferred rapidly from the N<sub>2</sub>O chromophore to the metal cluster by IVR, rather than in a coherent multiphoton process. This IVR process allows energy to be repeatedly absorbed via the same fundamental transition. Indeed, the efficiency of the argon-tagged experiments illustrates that IVR rates between N<sub>2</sub>O and the cluster must be fast on the time scale of the experiment.

The infrared driven surface chemistry described above represents a cluster analogue of temperature-programmed reaction studies on extended surfaces. In such experiments, N<sub>2</sub>O has been observed to adsorb molecularly at low temperatures but decomposes releasing N<sub>2</sub> when heated above ca. 100 K, the exact temperature depending on the crystal surface.<sup>40</sup> In an attempt to further test the idea of a thermal mechanism in the cluster case, we have performed similar experiments on Rh<sub>n</sub>ON<sub>2</sub>O<sup>+</sup> complexes to those described above for Rh<sub>n</sub>N<sub>2</sub>O<sup>+</sup>. The results for Rh<sub>6</sub>ON<sub>2</sub>O<sup>+</sup> are shown in Figure 6 and show that N<sub>2</sub>O decomposition occurs not only when the cluster is heated via the nitrous oxide vibrational modes (such as the bend around 560 cm<sup>−1</sup>) but also following pumping the O-stretch at 620–650 cm<sup>−1</sup>. The presence of coadsorbed O atoms does, however, subtly affect the surface chemistry in ways which will be described in detail elsewhere.<sup>48</sup> For the present purposes, it is sufficient to say that the observed surface chemistry can clearly be driven using an alternative chromophore to the N<sub>2</sub>O ligand, thus supporting the idea of it being a thermal process. Following this logic it should be possible to drive the chemistry by pumping the low frequency metal cluster modes directly (see below). However, the sheer number of photons which would need to be absorbed, coupled with the much smaller absorption cross sections of these transitions, makes this process highly unlikely and probably explains why no such process was observed in this study.

**Low Frequency Vibrational Modes.** Below 350 cm<sup>−1</sup> the Rh<sub>n</sub>N<sub>2</sub>OAr<sup>+</sup> spectra are dominated by transitions identifiable with vibrational modes within the rhodium cluster frameworks. Several transitions are observed for cluster sizes 5 ≤ *n* ≤ 8 in this spectral region although all of them are very much weaker than those related to the N<sub>2</sub>O moiety. It is generally the case that the spectra in these regions differ markedly from those of the naked Rh<sub>n</sub><sup>+</sup> clusters<sup>21</sup> in terms of both the number and intensities of observed transitions reflecting the significant perturbation which the adsorption of the N<sub>2</sub>O has on the naked cluster structure and the increased dipole moment resulting in some modes. In the same way as has been done with naked clusters, the spectra in this region can be compared with the calculated spectra of the low-lying isomers identified by the computational search.

Figure 7 shows a comparison of the low frequency region of the Rh<sub>5</sub>N<sub>2</sub>OAr<sup>+</sup> and Rh<sub>6</sub>N<sub>2</sub>OAr<sup>+</sup> spectra with simulated spectra



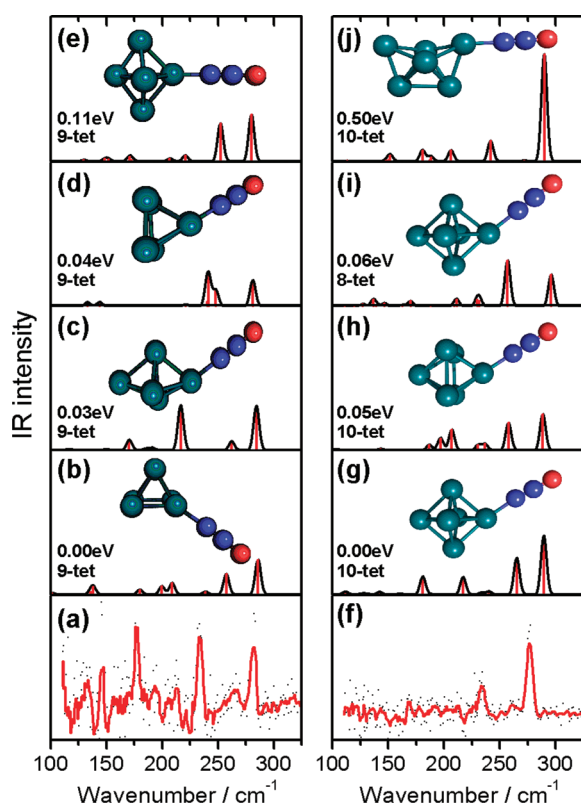


**Figure 7.** (a) IR-MPD spectrum of  $\text{Rh}_5\text{N}_2\text{OAr}^+$  in the region of the metal–metal modes. (b–e) The calculated spectra of the four lowest-lying isomers identified for  $\text{Rh}_5\text{N}_2\text{O}^+$ . (f) IR-MPD spectrum of  $\text{Rh}_6\text{N}_2\text{OAr}^+$  in the region of the metal–metal modes and (g–j) calculated spectra of the four lowest-lying isomers identified for  $\text{Rh}_6\text{N}_2\text{O}^+$ .

of the four lowest energy structures identified for each. The experimental spectrum of  $\text{Rh}_5\text{N}_2\text{OAr}^+$  in this region is particularly weak, but even so at least three identifiable peaks are observed. The lowest-lying calculated structures are based on square-based pyramidal and trigonal bipyramidal  $\text{Rh}_5^+$  motifs with spin multiplicities  $(2S + 1) = 9$ . None of the individual calculated spectra provides a particularly convincing match with the experimental spectrum, though we cannot preclude the possibility of multiple states/isomers being present.

The IR-MPD spectrum of  $\text{Rh}_6\text{N}_2\text{O}^+$  comprises only two significant peaks suggesting a relatively high symmetry structure. This is reflected in the lowest lying calculated structures, all of which ( $<0.5$  eV) are based on an octahedral (strictly a distorted square-based bipyramid)  $\text{Rh}_6$  motif with spin multiplicity 10 (g,h) or 8 (i). Of these, the octet octahedron (Figure 7i), provides the best match to the experiment. While this is consistent with the assignment of the bare cluster structure,<sup>21</sup> a reasonable fit is, however, also provided by the boat structure, (Figure 7j) calculated to lie 0.5 eV above the lowest energy calculated structure. Such a higher lying isomer could account for the observation of multiple reactivities for this cluster size.<sup>3,6</sup>

Figure 8 shows a similar comparison of experimental and simulated IR-MPD spectra for  $\text{Rh}_7\text{N}_2\text{OAr}^+$  and  $\text{Rh}_8\text{N}_2\text{OAr}^+$ . In the case of naked  $\text{Rh}_7^+$ , all low-lying isomers were calculated to be pentagonal bipyramidal and these form the basis for the  $\text{Rh}_7\text{N}_2\text{O}^+$  structures determined in this study. The putative global minimum is found to be an 11-tet in which  $\text{N}_2\text{O}$  binds atop an axial rhodium atom. Beyer and Knickelbein measured an

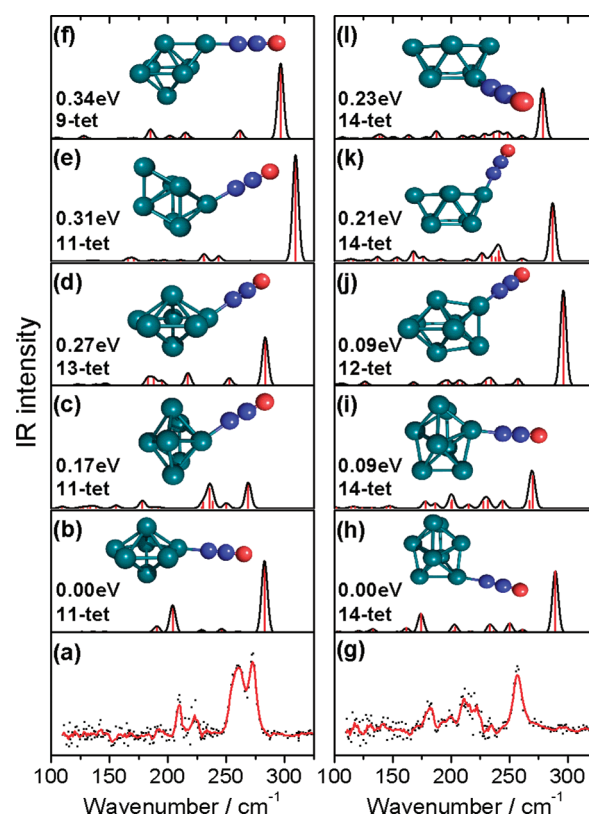


**Figure 8.** (a) Measured IR-MPD spectra of  $\text{Rh}_7\text{N}_2\text{OAr}^+$  and calculated (b–f) IR-MPD spectra of  $\text{Rh}_7\text{N}_2\text{O}^+$  in the region of the metal–metal modes. (g) Measured IR-MPD spectra of  $\text{Rh}_8\text{N}_2\text{OAr}^+$  and calculated (h–l) IR-MPD spectra of  $\text{Rh}_8\text{N}_2\text{O}^+$  in the region of the metal–metal modes.

anomalously high electric dipole moment for neutral  $\text{Rh}_7$ , which may be explained by a capped-octahedral structure.<sup>49</sup> However, in both our earlier study of naked  $\text{Rh}_7^+$  and here, we calculate these structures to lie significantly higher in energy.<sup>21</sup> The measured IR-MPD spectrum of  $\text{Rh}_7\text{N}_2\text{O}^+$  exhibits two intense doublet features (common separation 13  $\text{cm}^{-1}$ ) to which no individual calculated spectrum provides a particularly good fit. The most intense feature in each of the calculated spectra is the Rh–N stretch, which is the highest frequency vibration in this region. It is tempting to propose the presence of two isomers; however, no definitive assignment is possible.

Our calculations on  $\text{Rh}_8\text{N}_2\text{O}^+$  with the TPSSH functional predict the most stable isomers to be based on bicapped octahedral structures, in agreement with our earlier IR-MPD study on the naked  $\text{Rh}_8^+$  cluster.<sup>21</sup> Clusters built on bicapped trigonal prism motifs lie around 0.2 eV higher (Figure 8k,l) with other structures, including the cube and diamond geometries (not shown), predicted to lie at least 0.6 eV above the global minimum. The experimental spectrum shows some similarity with the calculated spectra but a lack of distinguishing features precludes conclusive assignment.

Finally, in each of the experimental spectra shown in Figure 1 two peaks are observed in the 430–450  $\text{cm}^{-1}$  region, which cannot be assigned to vibrations of the rhodium cluster framework or to molecularly bound  $\text{Rh}_n\text{N}_2\text{O}^+$ . Closer investigation of these features reveals them to be artifacts arising from the presence of weak third and fifth harmonics of the FELIX fundamental that excite the N–O and N≡N stretches, respectively, which both have high IR intensities.



## CONCLUSIONS

IR-MPD spectroscopy using the inert atom messenger technique has shown that nitrous oxide can be molecularly adsorbed on the surface of cationic rhodium clusters,  $\text{Rh}_n^+$  ( $n = 4-8$ ). By comparison with structures and spectra calculated using density functional theory, it is possible to assign the  $\text{N}_2\text{O}$  to be atop bound via the terminal N atom, in a linear configuration on the rhodium cluster.

Cluster surface reactivity, resulting ultimately in the decomposition of the adsorbed  $\text{N}_2\text{O}$  moiety and generation of the corresponding oxide cluster, is induced by infrared multiple-photon absorption via the vibrational modes of the  $\text{N}_2\text{O}$  molecule. This reaction proceeds on all clusters studied with the notable exception of  $n = 5$ , a process which is shown to be thermally driven, via the cluster–O stretch in  $\text{Rh}_n\text{O}(\text{N}_2\text{O})^+$  clusters.

Difficulties encountered in definitively assigning the underlying cluster geometry highlight the challenges in applying exchange-correlation functionals, optimized for main group chemistry, to transition metal cluster–ligand systems. For these rhodium clusters, some proportion of HF exchange is apparently needed to obtain cluster geometries that are consistent with experiment, but too much HF exchange overestimates the cluster–ligand binding energy, contradicting the experimental evidence. The TPSSH functional was found to be the best compromise for calculating cluster geometries and reaction energies that support the experimental results. This functional was used to calculate a plausible reaction pathway, which involves rearrangement on the surface of the cluster to produce  $\text{Rh}_n\text{O}^+$  with concomitant loss of  $\text{N}_2$ .

## AUTHOR INFORMATION

### Corresponding Author

\*E-mail: felicke@fhi-berlin.mpg.de and stuart.mackenzie@chem.ox.ac.uk.

## ACKNOWLEDGMENT

We gratefully acknowledge the support of the Stichting voor Fundamenteel Onderzoek der Materie (FOM) for providing beam time on FELIX. The authors thank the FELIX staff for their skillful assistance, in particular Dr. B. Redlich and Dr. A. F. G. van der Meer. The Oxford participants are grateful to the EU FP7 programme ELISA for travel funding for their experimental runs at FELIX. We are grateful to Dr. D. M. Rayner for providing the rhodium rod and for insightful discussions of our results. This work was funded by EPSRC (EP/C012070) and was supported by the Cluster of Excellence “Unifying Concepts in Catalysis” coordinated by the Technische Universität Berlin and funded by the Deutsche Forschungsgemeinschaft. S.R.M. acknowledges the EPSRC for his Advanced Research Fellowship (EP/C01202X), W.S.H. the Ramsay Memorial Fellowships Trust in the form of a Ramsay Memorial Fellowship, and D.J.H. the Institute of Advanced Study, University of Warwick, and the Alexander von Humboldt Stiftung for support. T.R.W. and D.J.H. thank the Centre for Scientific Computing, University of Warwick, for computing resources. The authors would also like to acknowledge the use of the National Service for Computational Chemistry Software (NSCCS) and the Oxford Supercomputing Centre (OSC) in carrying out this work.

## REFERENCES

- (1) Somorjai, G. *Chemistry in Two Dimensions: Surfaces*; Cornell University Press: Ithaca, NY, 1981.
- (2) Zhdanov, V. P.; Kasemo, B. *Surf. Sci. Rep.* **1997**, *29*, 35.
- (3) Ford, M. S.; Anderson, M. L.; Barrow, M. P.; Woodruff, D. P.; Drewello, T.; Derrick, P. J.; Mackenzie, S. R. *Phys. Chem. Chem. Phys.* **2005**, *7*, 975.
- (4) Adlhart, C.; Uggerud, E. J. *Chem. Phys.* **2005**, *123*, 10.
- (5) Anderson, M. L.; Ford, M. S.; Derrick, P. J.; Drewello, T.; Woodruff, D. P.; Mackenzie, S. R. *J. Phys. Chem. A* **2006**, *110*, 10992.
- (6) Harding, D.; Ford, M. S.; Walsh, T. R.; Mackenzie, S. R. *Phys. Chem. Chem. Phys.* **2007**, *9*, 2130.
- (7) Armentrout, P. B. *Annu. Rev. Phys. Chem.* **2001**, *52*, 423.
- (8) Knickelbein, M. B. *Annu. Rev. Phys. Chem.* **1999**, *50*, 79.
- (9) Cox, A. J.; Louderback, J. G.; Apsel, S. E.; Bloomfield, L. A. *Phys. Rev. B* **1994**, *49*, 12295.
- (10) Cox, A. J.; Louderback, J. G.; Bloomfield, L. A. *Phys. Rev. Lett.* **1993**, *71*, 923.
- (11) Reddy, B. V.; Khanna, S. N.; Dunlap, B. I. *Phys. Rev. Lett.* **1993**, *70*, 3323.
- (12) Harding, D.; Mackenzie, S. R.; Walsh, T. R. *J. Phys. Chem. B* **2006**, *110*, 18272.
- (13) Harding, D. J.; Davies, R. D. L.; Mackenzie, S. R.; Walsh, T. R. *J. Chem. Phys.* **2008**, *129*, 7.
- (14) Majumdar, D.; Balasubramanian, K. *J. Chem. Phys.* **1998**, *108*, 2495.
- (15) Cramer, C. J.; Truhlar, D. G. *Phys. Chem. Chem. Phys.* **2009**, *11*, 10757.
- (16) Bae, Y. C.; Kumar, V.; Osanai, H.; Kawazoe, Y. *Phys. Rev. B* **2005**, *72*, 6.
- (17) Bae, Y. C.; Osanai, H.; Kumar, V.; Kawazoe, Y. *Phys. Rev. B* **2004**, *70*, 7.
- (18) Futschek, T.; Marsman, M.; Hafner, J. J. *Phys.: Condens. Matter* **2005**, *17*, S927.
- (19) Reddy, B. V.; Nayak, S. K.; Khanna, S. N.; Rao, B. K.; Jena, P. *Phys. Rev. B* **1999**, *59*, S214.
- (20) Wang, L. L.; Johnson, D. D. *J. Phys. Chem. B* **2005**, *109*, 23113.
- (21) Harding, D. J.; Gruene, P.; Haertelt, M.; Meijer, G.; Fielicke, A.; Hamilton, S. M.; Hopkins, W. S.; Mackenzie, S. R.; Neville, S.; Walsh, T. R. *J. Chem. Phys.* **2010**, *133*, No. 214304.
- (22) Harding, D. J.; Walsh, T. R.; Hamilton, S. M.; Hopkins, W. S.; Mackenzie, S. R.; Gruene, P.; Haertelt, M.; Meijer, G.; Fielicke, A. *J. Chem. Phys.* **2010**, *132*, No. 011101.
- (23) Hamilton, S. M.; Hopkins, W. S.; Harding, D. J.; Walsh, T. R.; Gruene, P.; Haertelt, M.; Fielicke, A.; Meijer, G.; Mackenzie, S. R. *J. Am. Chem. Soc.* **2010**, *132*, 1448.
- (24) Oepts, D.; Vandermeer, A. F. G.; Vanamersfoort, P. W. *Infrared Phys. Technol.* **1995**, *36*, 297.
- (25) Fielicke, A.; Kirilyuk, A.; Ratsch, C.; Behler, J.; Scheffler, M.; von Helden, G.; Meijer, G. *Phys. Rev. Lett.* **2004**, *93*, No. 023401.
- (26) Fielicke, A.; von Helden, G.; Meijer, G. *Eur. Phys. J. D* **2005**, *34*, 83.
- (27) Fielicke, A.; von Helden, G.; Meijer, G.; Pedersen, D. B.; Simard, B.; Rayner, D. M. *J. Phys. Chem. B* **2004**, *108*, 14591.
- (28) *TURBOMOLE V6.1*, 2009, a development of University of Karlsruhe and Forschungszentrum Karlsruhe GmbH, 1989–2007; TURBOMOLE GmbH, since 2007; available from <http://www.turbomole.com>, 1989–2007.
- (29) Banerjee, A.; Adams, N.; Simons, J.; Shepard, R. J. *Phys. Chem.* **1985**, *89*, S2.
- (30) Helgaker, T. *Chem. Phys. Lett.* **1991**, *182*, 503.
- (31) Mosch, C.; Koukounas, C.; Bacalis, N.; Metropoulos, A.; Gross, A.; Mavridis, A. *J. Phys. Chem. C* **2008**, *112*, 6924.
- (32) Perdew, J. P.; Ernzerhof, M.; Burke, K. *J. Chem. Phys.* **1996**, *105*, 9982.
- (33) Staroverov, V. N.; Scuseria, G. E.; Tao, J. M.; Perdew, J. P. *SJ. Chem. Phys.* **2003**, *119*, 12129.

- (34) Fielicke, A.; Gruene, P.; Haertelt, M.; Harding, D. J.; Meijer, G. *J. Phys. Chem. A* **2010**, *114*, 9755.
- (35) Jensen, K. P. *J. Phys. Chem. A* **2009**, *113*, 10133.
- (36) Weigend, F.; Ahlrichs, R. *Phys. Chem. Chem. Phys.* **2005**, *7*, 3297.
- (37) Weigend, F.; Haser, M.; Patzelt, H.; Ahlrichs, R. *Chem. Phys. Lett.* **1998**, *294*, 143.
- (38) Swart, I.; de Groot, F. M. F.; Weckhuysen, B. M.; Rayner, D. M.; Meijer, G.; Fielicke, A. *J. Am. Chem. Soc.* **2008**, *130*, 2126.
- (39) Teffo, J. L.; Chedin, A. *J. Mol. Spectrosc.* **1989**, *135*, 389.
- (40) Liu, S. W.; Horino, H.; Kokalj, A.; Rzeznicka, I.; Imamura, K.; Ma, Y. S.; Kobal, I.; Ohno, Y.; Hiratsuka, A.; Matsushima, T. *J. Phys. Chem. B* **2004**, *108*, 3828.
- (41) Zeigarnik, A. V. *Kinet. Catal.* **2003**, *44*, 233.
- (42) Madey, T. E.; Avery, N. R.; Anton, A. B.; Toby, B. H.; Weinberg, W. H. *J. Vac. Sci. Technol., A* **1983**, *1*, 1220.
- (43) Avery, N. R. *Surf. Sci.* **1983**, *131*, S01.
- (44) Haq, S.; Hodgson, A. *Surf. Sci.* **2000**, *463*, 1.
- (45) Hussain, G.; Rahman, M. M. *Spectrochim. Acta, Part A* **2006**, *64*, 880.
- (46) Henderson, M. A.; Szanyi, J.; Peden, C. H. F. *Catal. Today* **2003**, *85*, 251.
- (47) Schroder, D.; Shaik, S.; Schwarz, H. *Acc. Chem. Res.* **2000**, *33*, 139.
- (48) Hermes, A.; Hopkins, W. S.; Hamilton, S. M.; Harding, D. J.; Kerpel, C.; Haertelt, M.; Meijer, G.; Fielicke, A.; Mackenzie, S. R. In preparation.
- (49) Beyer, M. K.; Knickelbein, M. B. *J. Chem. Phys.* **2007**, *126*, 7.